International Journal of Fatigue, Volume 32, Issue 4, April 2010, Pages 735-743

Accepted Manuscript

The effect of weld residual stresses and their re-distribution with crack growth during fatigue under constant amplitude loading

C.D.M. Liljedahl, O. Zanellato, M.E. Fitzpatrick, J. Lin, L. Edwards

PII: S0142-1123(09)00305-3
DOI: 10.1016/j.ijfatigue.2009.10.012
Reference: JIJF 2377

To appear in: *International Journal of Fatigue*

Received Date: 19 December 2008
Revised Date: 4 September 2009
Accepted Date: 19 October 2009

Please cite this article as: Liljedahl, C.D.M., Zanellato, O., Fitzpatrick, M.E., Lin, J., Edwards, L., The effect of weld residual stresses and their re-distribution with crack growth during fatigue under constant amplitude loading, *International Journal of Fatigue* (2009), doi: 10.1016/j.ijfatigue.2009.10.012

The effect of weld residual stresses and their re-distribution with crack growth during fatigue under constant amplitude loading

C. D. M. Liljedahl[1], O. Zanellato[1], M. E. Fitzpatrick[1,*] J. Lin[2], and L. Edwards[1, 3]

[1] Materials Engineering, The Open University, Walton Hall, Milton Keynes, MK7 6AA, UK

[2] Damage Tolerance Group, Cranfield University, Bedfordshire MK43 0AL, UK

[3] Currently at Australian Nuclear Science and Technology Organisation, PMB1, Menai, NSW 2234, Australia

*Corresponding author: m.e.fitzpatrick@open.ac.uk

Abstract

In this work the evolution of the residual stresses in a MIG-welded 2024-T3 aluminium alloy M(T) specimen during in-situ fatigue crack growth at constant load amplitude has been measured with neutron diffraction. The plastic relaxation and plasticity-induced residual stresses associated with the fatigue loading were found to be small compared with the stresses arising due to elastic redistribution of the initial residual stress field. The elastic redistribution was modelled with a finite element simulation and a good correlation between the experimentally-determined and the modelled stresses was found. A significant mean stress effect on the fatigue crack growth rate was seen and this was also accurately predicted using the measured initial residual stresses.

Keywords: *Neutron diffraction, residual stresses, fatigue, welding, finite element analysis*

1. Introduction

Accounting for the effects of metal fatigue plays a major role in the design of optimized aerospace structures [1], as the constraints of reduced cost and increased design life of structures have changed the way new materials are introduced in the design cycle of new products. Aircraft design has moved from a purely performance-driven design approach to an approach which incorporates improved performance, extended operating life and reduced environmental impact of the aircraft structure [2].

Using large integral structural sections in the design of aerospace components can significantly reduce the weight of the final assembly. Such structures use new manufacturing methods, as for instance friction-stir welding, which replaces conventional joining methods such as riveting and bolting. However, unlike riveted structures, welded structures typically contain no crack stoppers that can retard or arrest fatigue crack propagation. Another inherent inconvenience with welds is the residual stresses caused by the intense local heating. These stresses can significantly influence the fatigue life of engineering components [3-6]. Fail-safety and damage-tolerance regulations hence impose large safety factors where residual stresses may be present, and this reduces the weight competitiveness of integral structures. Thus, lifing models have to be verified in order to be able to fully exploit the advantages of welded integral structures.

The linear elastic fracture mechanics method is the most frequently employed approach to account for the effect of an existing residual stress field on fatigue crack growth behaviour [7]. It is assumed that the principle of superposition is valid and that residual

stress redistribution is not affected by the presence of the small-scale plasticity associated with fatigue crack growth [8]. However, whilst allowing final crack growth lives to be predicted with reasonable accuracy, the form of the crack length versus load cycles curve is typically quite different from the test results, with initial crack growth being underestimated and later crack growth being overestimated [9, 10].

Therefore, detailed knowledge of the evolution of residual stresses with fatigue crack growth therefore has to be determined to assess and validate such models. Several researchers[11-14] have attempted to measure the residual stress relaxation that occurs with crack growth. However, in the above papers the 'crack' was extended by machining a notch in the specimen. Under these circumstances, elastic redistribution of the stress is expected and observed since the slot produced does not have the plasticity associated with a fatigue crack. In addition, a machined notch, in contrast to a fatigue crack, cannot withstand a compressive traction and as a consequence, elastically relieves a compressive residual stress.

Several researchers [15-18] have investigated the influence of the microstructural changes caused by welding procedures in various materials. These studies revealed that these changes have a relatively small influence on the fatigue crack growth rate.

It has been suggested that one of the reasons why lifetime prediction in the presence of a strong residual stress fields is difficult is because of the residual stress redistribution that

occurs due to the interaction between the plasticity that accompanies the fatigue crack and the misfit strains that induced the original residual stress field [10, 19].

Neutron diffraction has been used for measurement of residual stresses in various types of materials and industrial components [20-22]. The method has been extensively applied to measure residual stresses in welds [23-27] as the stresses are usually high, the gauge volume typically used is small compared to the weld and the penetration depth of the neutron beam into the material is large. Furthermore, the method is non-destructive at the point of application and is therefore ideal for the monitoring of residual stress fields in fatigued samples (although some components require the machining of access channels [28] and welds require the determination of a point-to-point stress-free lattice reference which requires extraction of material from the weld being measured or an identical component [29]).

In previous work by the authors of this paper it has been shown by measurement and modelling that the evolution of the residual stresses in a welded M(T) and C(T) specimen loaded at constant ΔK is governed by elastic redistribution [30, 31]. It was further shown that if the initial residual stresses are known, the effect of the residual stresses on the fatigue crack growth rate can be predicted using a fracture mechanics approach [32].

The focus of the present work is to investigate if the residual stresses are governed by elastic redistribution also for a specimen loaded at constant load amplitude, *i.e.* with increasing stresses intensity factor and plastic deformation at the crack tip as the crack

length increases. Plastic deformation might cause a difference in the weld residual stress redistribution and relaxation which may invalidate the assumption of superposition.

In this work, the residual stresses were measured with neutron diffraction *in-situ* during fatigue loading at the SALSA diffractometer of the ILL neutron source in Grenoble, France[33]. The re-distribution and the effect of the residual stresses on the crack tip stress intensity factor were predicted with a finite element simulation and Green's functions. The fatigue crack growth rate through the weld was then predicted by accounting for *R*-ratio effects induced by the residual stresses, in conjunction with empirical fatigue crack growth rate curves.

2. Experimental procedures

The material and the specimens' manufacture is presented in Section 2.1. In Section 2.2 the procedures and the details of the residual stress measurements and the fatigue crack testing are given.

2.1 Material and specimen preparation

Metal-inert-gas (MIG) welding was used to manufacture 2024 aluminium plates 500 mm × 500 mm. The plates were welded with the weld direction parallel to the longitudinal plate orientation. Aluminium alloy 2024, heat treated to T351 specification, was used. A number of plates were welded, using nominally identical conditions, by the Welding Research Centre at Cranfield University, UK. The welding was carried out in two passes

with a travel speed of 450 mm min^{-1}. The current and voltage used in the MIG welding process were 268 A and 24.3 V respectively. After welding the plate was skimmed down to 7 mm and the middle tension (M(T)) specimens were machined with the dimensions and orientations as shown in Fig. 1, according to ASTM E 647-00. An initial 'defect' with total length ($2a$) of 6.7 mm was machined on the weld line using Electro-Discharge Machining (EDM).

2.1 Neutron diffraction and fatigue testing

Neutron diffraction is an established non-destructive technique for determination of strains within metallic structures[20]. The inter-planar distance can be determined from the position of the diffraction peaks as realized by Bragg[34]:

$$d = \frac{\lambda}{2\sin\theta} \tag{1}$$

where d is the inter-planar distance, λ is the wavelength of the scattering neutrons and θ is the angle between the incident ray and the scattering planes. The direct strain (ε) in the material in the measured direction can henceforth be computed if both the inter-planar distance of the stressed component (d_σ) and an unstressed reference sample (d_0) are measured, using the following expression:

$$\varepsilon = \frac{d_\sigma - d_0}{d_0} = \frac{\sin\theta_0}{\sin\theta_\sigma} - 1 \tag{2}$$

The neutron diffraction measurements were carried out on the SALSA diffractometer[33] at the Institute Laue-Langevin in Grenoble, France. Aluminium is FCC (face centred cubic), and measurements were made using the {311} plane, as it gives a high

multiplicity and the elastic response of the {311} plane has been shown to correlate well with the macroscopic elastic response [35]. The wavelength was set to 1.7 Å (0.17 nm) to achieve a nearly cubic gauge volume by having a scattering angle (2θ) close to 90º.

The stress-free lattice parameter can vary significantly in both the heat affected zone and in the weld material itself [36]. Thus, a stress-free reference comb sample was machined using EDM from sections of the original welded plate. The dimensions of the comb teeth (2.4 mm × 9 mm × 2.7 mm) were small enough to assure that they were virtually stress-free [37]. The inter-planar distance could hence be determined as a function of the distance from the weld centre. The gauge volume used for the stress-free sample was 1 mm × 5 mm × 1 mm, with the longer dimension in the through-thickness direction to ensure that gauge volume was entirely within the 'fingers' of the comb.

The specimen was oriented edge-on to the neutron beam (Fig. 2), which is rotated 90˚ from the usual orientation which would be used to perform neutron diffraction measurements of the longitudinal strain component in a plate specimen. Although this increases the neutron beam path length through the specimen, it allows the use of a gauge volume that extends through the thickness of the specimen (there is no spurious peak shift due to having the gauge volume partially outside the sample in the vertical direction), so reducing measurement times. The sample is relatively thin, tending towards plane stress rather than plane strain conditions, and no significant stress gradient is expected through the thickness [26]. Both the incoming and the receiving slits were set to 2 mm horizontally, and through the whole specimen thickness vertically. Aluminium has a

relatively low neutron cross section and therefore the ~115 mm path length does not unduly affect the counting time, and measurements of lattice parameter to an accuracy of about 40 με (40×10^{-6}) could be achieved in 3 minutes.

Reference measurements were also carried out on a pure aluminium powder using the two different gauge volumes to be able to determine the small peak shift (<200 με) which occurred when the slits were altered for the measurements on the stress-free comb.

Before fatiguing the specimen the residual stresses were measured along a line 55 mm from the notch, as indicated in Fig. 1, to obtain the initial and un-cracked stress distribution.

The evolution of the residual stresses with fatigue crack growth was then measured by fatigue loading the specimen *in-situ* on the diffractometer. This was achieved by fixing a 100 kN Instron servohydraulic stress rig on the SALSA sample table (Fig. 2). A sinusoidal shape was used for the load cycle with a maximum load of about 60 MPa and an *R*-ratio (ratio between the minimum and maximum load) of 0.1. The initial frequency was set to 10 Hz. As the fatigue crack growth was undertaken *in situ* in the neutron beam neither optical nor potential drop monitoring of crack length was feasible, and therefore the crack length was monitored with a fractomat gauge (FAC-20, Tokyo Sokki Kenkyojo Co., Ltd.). More precise crack growth measurements were also carried out on nominally identical specimens on laboratory fatigue machines using potential drop crack length measurement.

The residual stresses were measured along the crack growth direction through the entire width of the specimen. The specimen was fatigued to grow the crack and then the specimen was un-loaded and the residual stresses were measured. After measurement in one direction the sample table was rotated 90º with the stress rig still fixed on top for measurement in the other (transverse) strain direction. This was repeated until a final crack length of 26 mm was reached. The applied ΔK increased during the test from 5.6 MPa√m at the initial notch to 22 MPa√m at the final crack length. The stress ratio R was 0.1.

The majority of the strain measurements were taken at zero load, *i.e.*, only residual stresses were determined. However, for some crack lengths, strains were also measured with the sample held at the maximum load in the fatigue cycle (P_{max}).

Plane stress conditions were assumed to exist in the plate, as the thickness was small compared with the width, and hence only the longitudinal and the transverse components had to be measured for computation of the residual stresses using the generalized form of Hooke's law:

$$\sigma_i = 2\mu\varepsilon_i + \lambda\sum_i \varepsilon_i \ (i = 1,2,3)$$

where $\mu = \frac{E}{2(1+\nu)}$, $\lambda = \frac{\nu E}{(1+\nu)(1-2\nu)}$, and $E = 72$ MPa and $\nu = 0.33$ for the Al alloy.

3. Experimental results

3.1 Comb measurements

The variation of 2θ in the longitudinal and transverse directions in the stress-free comb sample is given in Fig. 3. It can be seen that there is a significant change in stress-free lattice spacing in the transition between the weld and parent material. The variation in both directions was similar, and this indicates that the reference samples were indeed stress-free. The difference seen between the two directions is indicative of some direction-dependence of the strain-free values, probably as a result of texture in the plate, which is generally a consequence of the rolling method used in its production. The variability in the parent material is also indicative of texture effects. However, the maximum difference between the two directions is relatively small, <90 με.

3.2 Measured evolution of residual strains and stresses with crack extension

The strain values at each measurement position were computed using the measured 2θ in the stress free comb and the measured 2θ in the welded M(T) specimen (equation 2). The un-cracked and un-fatigued strain and stress distributions, along the uncracked line A-A' as shown in figure 1, are shown in Figures 4a and 4b respectively.

Lefebvre *et al*. have [38] measured the residual stresses in a specimen of the same material with similar dimensions, using near-surface X-ray diffraction, and found that the peak residual stresses were about 170 MPa. This is consistent with the values measured in this study in the bulk of the sample (Fig. 4b).

The residual stresses arise due to non-uniform expansion and contraction caused by the local heating during welding. The hot weld material yields easily, and on cooling down misfit strains are caused between the yielded and the un-yielded material. This induces large stresses parallel to the weld line (the longitudinal direction). As in most welds, tensile stresses exist in the regions close to the weld line and are balanced by compressive stresses further out. The microstructural changes that occur in the weld and HAZ (heat affected zone) of this precipitation-hardened aluminium alloy produce a double residual stress peak on each side of the weld [25] as is seen in Fig. 4b.

Only the longitudinal residual stresses will be discussed in this paper, as they will be primarily responsible for affecting the Mode I fatigue crack growth in this sample geometry.

The full evolution of the longitudinal stresses, together with the Finite Element simulation results that will be described later are shown in Figures 5 (a) to (e). The uncertainty in measurement was calculated for each point but it is not plotted in these figures to allow for clearer visualization of the data. The stress uncertainties, calculated from the uncertainty in the fit to each diffraction peak, were around ±7 MPa.

It can be seen that the peak residual stress increases with crack growth until a crack length of about 14 mm from the weld centre. It can also be seen that the compressive region of the residual stress away from the crack tip is initially unaffected by the crack growth. Once the magnitude of the tensile stresses around the crack tip starts to decrease, the magnitude of the compressive stress also decreases to remain in equilibrium (Fig. 5).

The residual stresses are compared with the stresses measured in the specimen when loaded to P_{max} in Fig. 6 (a) to (e). Here it can be seen that the residual stresses are larger in the tensile region than the stresses induced by the applied load until the crack length is about 20 mm. It should be noted that the peak residual stresses increase with crack length until about 14 mm, whereas the applied ΔK increases continuously with the crack length. The measured compressive residual stress field in the wake of the crack (behind the crack tip position) for the M(T) specimen (Fig. 4a) was independent of applied load and therefore cannot be due to physical crack closure. Tsakalakos *et al*.[39] and Croft *et al*.[40] have measured the residual strain within a fatigued C(T) specimen subjected to a single overload cycle using energy-dispersive synchrotron X-ray diffraction. They also found an apparent compressive stress in the wake of the crack (behind the crack tip) even after the specimen was completely fractured; hence again there is no physical closure. Compressive macro-stresses can be ruled out as the crack plane must be a traction-free surface. These authors suggested that these apparent stresses may be due to anisotropic plastic strains in the crack wake [40] or measurement error owing to the gauge volume differing in the two measured directions [39]. The assumption of plane stress may also have induced some errors in the computation of the stress, but performing the calculation using a plane strain assumption only affects the magnitude of the calculated stresses (with higher magnitudes in plane strain) and does not affect their sign.

3.3 Fatigue crack rate through the specimen

The measured crack growth rate through the specimen, made on laboratory fatigue machines using potential drop crack length measurement carried out at Cranfield University, is shown in Fig. 7. This data was generated with exactly the same cyclic loads as the specimen tested at SALSA, i.e. ΔP = 30.34 kN, P_{max} = 33.71 kN and R = 0.1.

4. Residual stress modelling

The commercial finite element (FE) code ABAQUS (standard version 6.5) was used for all the FE modelling. The plate was thin compared to the width and the gauge volume extended through the whole thickness, so plane stress conditions were assumed. Plane stress, 8 noded elements (CPS8) with full integration was used throughout this study. The smallest elements along the crack plane were 0.125 × 0.125 mm^2.

Two approaches were employed to introduce the measured residual stresses in the M(T) specimen FE models. The first is the eigenstrain approach [41]. Eigenstrain (ε^*) is the non-uniform inelastic strain which causes elastic residual strains and hence stresses. Where the residual stresses are known throughout the whole component, then ε^* can be determined from the following relation directly:

$$\varepsilon^* = -C_{ijkl}^{-1}\sigma_{kl}^{RS} \tag{3}$$

where C is the elastic constant tensor and σ^{RS} are the measured residual stresses.

The stress distribution ahead of the notch was measured in the M(T) specimen before it was fatigued (Figure 5a). This stress distribution was assumed to represent the

distribution throughout the un-cracked specimen (*i.e.*, assuming that the welded plate was continuously-processed). In this case, for a continuously-processed body with 2D symmetry, one eigenstrain component in the longitudinal direction will contribute to the residual stresses[42] as the other components satisfy the compatibility equation. The transverse stress will also be small in the un-cracked component. The eigenstrain was hence computed as follows:

$$\varepsilon_{11}^{*}(y) = -\frac{\sigma_{11}^{RS}(x)}{E} \tag{4}$$

where E is the Young's modulus for the material. The eigenstrain field was introduced into the FEA model using a pseudo-anisotropic thermal strain: the UEXPAN subroutine available in ABAQUS is used to define an orthotropic coefficient of thermal expansion as a function of position. The coefficient of thermal expansion was set to the value of the eigenstrain at each point and a unit temperature load was then applied to introduce the required inelastic strain.

For comparison, the residual stress field was read in directly into the model using the SIGINI FORTRAN subroutine implemented in ABAQUS. This is the second approach taken for modelling the residual stress distribution. In the first step of this analysis, the stresses were allowed to equilibrate, simulating the residual stresses in the M(T) specimen.

The resulting initial residual stresses using both the SIGINI subroutine and the eigenstrain approaches are shown in Fig. 8. There is an extremely good correlation between the two sets of FE results, and good agreement with the measured data.

Crack extension was then modelled by removing the boundary conditions along the symmetry line. In order to be able to compare the predictions with the experimental results, the stresses were averaged over those elements equivalent to the measured gauge volume to be able to compare the numerical results with the values obtained experimentally. The stresses averaged over the gauge volume converged readily despite the stress concentration at the crack tip (Fig. 9).

The predicted elastic re-distribution with crack growth is shown in Fig. 5. The predicted stresses when the specimen was loaded are shown in Fig. 6.

5. Modelling of the fatigue crack growth behaviour

The evolution of the residual stress intensity factor with crack growth has to be computed in order to be able to predict the effect of the residual stresses on the fatigue crack growth rate. Two methods were used: Green's functions, and a finite element approach. The predicted fatigue crack growth rate through the material was calculated using empirical fatigue crack growth curves.

5.1 The evolution of the residual stress intensity factor

Green's functions

The residual stress intensity factor (K_{res}) is most commonly determined from weight and Green's functions (h(x, a) using the initial un-cracked residual stress distribution, as derived by Bueckner[43]:

$$K_{res}(a) = \int_{-a}^{+a} h(x,a)\sigma_{res}(x)dx \tag{5}$$

where a is the crack length at which K_{res} is computed and σ_{res} is the initial residual stress distribution.

Kanazawa's[44] Green's function for a crack growing from the centre of a plate, which accounts for finite width, is:

$$h(x,a) = \left[\frac{2\sin\frac{\pi(a+x)}{W}}{W\sin\frac{2\pi}{W}\sin\frac{\pi(a-x)}{W}} \right]^{\frac{1}{2}} \tag{6}$$

where W is the plate width of the specimen. The resulting residual stress intensity factor with increasing crack length is shown in Fig. 10.

Contour interaction method

The evolution of the residual stress intensity factor with crack growth was also determined with a finite element approach. The initial residual stresses were read into the model as explained in Section 4, and the crack growth was simulated by removing the symmetry boundary conditions. The stress intensity factor was determined through the contour interaction method implemented in ABAQUS. The contour interaction method is similar to the J-Integral method[45], but the stress intensities in each mode can be subtracted which is not the case with the J-Integral method.

The finite element results are compared with the results from the Green's function solution in Fig. 10. There is very good correlation between the two solutions.

5.2 Fatigue crack growth rate

The effect of the residual stresses on the fatigue crack growth rate is often predicted either with a superposition approach or with a crack closure approach. The crack closure approach has been shown not to yield good predictions of the effect of tensile residual stresses at low to intermediate applied constant stress intensity factors, as the contribution of any crack closure is very small in this case and hence very difficult to measure[46].

It has further been shown that, for positive R (K_{min}/K_{max}) in the case of positive residual stress intensity factors, the crack is opened further by the residual stresses and superposition is valid as no crack surface interactions occur as would be the case for a compressive residual stress field[32].

In this study, there is a high tensile residual stress field present and hence the superposition approach was used.

The superposition approach for prediction of the effects of the residual stress involves computation of the residual stress intensity factor (K_{res}) and then superposition of this to the stress intensity factor from the external loading (K_{load}), as follows:

$$K_{\max} = K_{\text{load/max}} + K_{\text{res}}$$
$$K_{\min} = K_{\text{load/min}} + K_{\text{res}} \quad (7)$$

The stress intensity range (ΔK) and stress ratio (R) is then computed as[47]:

$$\Delta K = K_{\max} - K_{\min} \left[= K_{\text{load/max}} - K_{\text{load/min}}\right], \quad R = \frac{K_{\min}}{K_{\max}} \quad (8)$$

In this approach only R changes and ΔK remains unaffected by the residual stresses. The applied ΔK for an M(T) specimen with the dimensions given in Figure 1 and loaded at a maximum load of 60.2 MPa and an R of 0.1 is given in Fig. 11a (standard solution for a through-crack) . The evolution of R is compared with the externally-applied R in Fig. 11b. It can be seen that a considerable mean stress effect can be expected.

The fatigue crack growth rate was predicted using the NASGRO equation. The NASGRO equation, which is effectively an empirical Paris-type relation in a sigmoid form where the R effect in included as in the given in the expression below (equation 8):

$$\frac{da}{dN} = \left[C\left(\frac{1-f}{1-R}\right)\Delta K\right]^n \frac{\left(1-\frac{\Delta K_{th}}{\Delta K}\right)^p}{\left(1-\frac{K_{\max}}{K_{crit}}\right)^q} \quad (9)$$

where C, n, p, q and f are empirical material parameters. The relevant material constants for 2024-T351 are available in the AFGROW database[48]. The predicted fatigue crack growth rate through the weld residual stress field can be seen in Fig. 7. The data is compared with prediction of the FCGR without including the effect of the residual stresses. It can be seen that the residual stresses accelerate the fatigue crack growth rate considerably.

6. Discussion

In prior work [28] the residual stress re-distribution in a VPPA-welded M(T) specimen was investigated. In that work the specimen was loaded at constant ΔK = 6 MPa$\sqrt{m}$. The macroscopic stress redistribution also appeared to be elastic in that case. The current experiment was mainly carried out to investigate if this also was valid for a MIG weld, but more importantly whether a specimen loaded with a constant load – *i.e.*, increasing ΔK with crack length – would show residual stresses re-distribution governed by the elastic re-distribution of the initial residual stress field or be affected by the plasticity induced during.

The measured residual stresses were seen to initially increase with crack length and then at long crack lengths to decrease (Fig. 5). The modelled elastic redistribution of the initial residual stress field showed the same characteristics. This indicates that the residual stress distribution with fatigue crack growth is governed by elastic redistribution, and that the local crack tip stresses and the associated plastic zone have a minor significance, at least at this level of resolution.

The measured residual stress peaks were seen to be slightly further out from the weld centre than the modelled stresses (Fig. 5). This might be due to the effect of crack tip plasticity, which pushes the peaks stresses forward[30]. There may also be an effect because the crack length was measured with Fractomat gauges, which is not a precision

technique. The slight overestimation of the peak stresses might also be due to plastic effects which were not included in the FE model. Plasticity was not included as one of the objectives of this study was to investigate if linear elastic fracture mechanics can be used in the prediction of the FCGR in the presence of a strong residual stress field.

The apparent compressive stress in the wake of the crack must however be due to a measurement error, as the these stresses are not relieved when the specimen is loaded to the maximum load in the fatigue cycle (Fig. 6). From this figure it can also been seen that elastic superposition seems to be valid as modelling and the measurement are in good correlation. The stresses in an identical specimen without residual stresses at the maximum load at the fatigue cycle were estimated by subtracting the measured stresses at P_{max} with the stresses at zero load. The good agreement with the modelled stresses in the body at the maximum load without any residual stresses and this estimate also indicates that elastic superposition is valid.

However, it has to be highlighted that when referring to plasticity effects on the residual stresses, the important condition in this context – the effect on the fatigue crack growth behaviour – is that the plasticity does not re-distribute the residual field differently compared with stress arising from an external load. It is therefore only necessary to implicitly include plasticity by use of the empirical fatigue crack growth laws derived from fatigue data where plasticity is obviously present.

The residual stresses would be expected to induce a significant mean stress effect and this is seen as an accelerated fatigue crack growth rate in the M(T) specimen compared with the parent material data (Fig. 7).

This increase was also expected, as both the Greens function and FE models of the residual stress intensity factor evolution with crack extension showed a high positive value (Fig. 9). It can also been seen that the relation between the difference between the measured stresses at the maximum load and the residual stresses in the unloaded condition (Fig. 6) is in the same order of magnitude as the relation between the applied stress intensity factor (Fig. 10a) and the residual stress intensity factor (Fig. 9). This reinforces the validity of the residual stress intensity factor computation.

The predicted FCGR in the welded M(T) specimens agreed well with the experimental results. The solution was however slightly conservative, and more so at shorter crack lengths. This might be due the microstructural changes in the weld and in the transition between the HAZ and the parent material, which are not included in the model at this time.

7. Concluding remarks

1. Neutron diffraction has been used to measure the evolution of residual stress as a crack is grown through a weld residual stress field, at a constant load range (*i.e.*, increasing ΔK

as the crack grows). The results have been compared with the predicted stress relaxation from an elastic finite element model.

2. The effect of the weld residual stress field on fatigue crack growth rate has been predicted using FE and Green's function approaches. Improved correlation with the experimentally-observed crack growth rates is obtained when the residual stresses are included in the crack growth model.

3. The re-distribution of the residual stress field can be predicted with good accuracy using the assumption of elastic re-distribution only. Therefore the plasticity associated with the fatigue crack growth has only a minimal effect on the residual stress redistribution.

4. It can hence be concluded that the evolution of the residual stresses at this level of resolution are governed by elastic re-distribution even at constant load, and that linear elastic fracture mechanics can be used successfully in the assessment of the fatigue behaviour if the initial residual stress field in the component is known.

Acknowledgements

CDML is grateful for financial support to Airbus UK, Alcoa and Cytec. The authors gratefully acknowledge the assistance of instrument scientist Dr D. J. Hughes at the SALSA diffractometer of the Institut Laue Langevin; and Mr P. Ledgard at Materials

Engineering, The Open University for manufacturing of the fatigue grips used. MEF is supported by a grant through The Open University from the Lloyd's Register Educational Trust, an independent charity working to achieve advances in transportation, science, engineering and technology education, training and research worldwide for the benefit of all.

References

[1] Molent L, Barter SA. A comparison of crack growth behaviour in several full-scale airframe fatigue tests. International Journal of Fatigue 2007;29(6):1090-1099.
[2] Williams JC, Starke EA. Progress in structural materials for aerospace systems. Acta Materialia 2003;51(19):5775-5799.
[3] Glinka G. Effect of Residual Stresses on Fatigue Crack Growth in Steel Weldments Under Constant and Variable Amplitude Loads. In: Fracture Mechanics, ASTM STP 677. Smith CW, editor.: ASTM, 1979, pp. 198-214.
[4] Itoh YZ, Suruga S, Kashiwaya H. Prediction of fatigue crack growth rate in welding residual stress field. Engng Fract Mech 1989;33(3):397-407.
[5] Shi YW, Chen BY, Zhang JX. Effect of welding residual stresses on fatigue crack growth behaviour in butt welds of a pipeline steel. Engng Fract Mech 1990;36(6):893-902.
[6] Lefebvre F, Sinclair I. Micromechanical aspects of fatigue in a MIG welded aluminium airframe alloy: Part 2. Short fatigue crack behaviour. Materials Science and Engineering: A 2005;407(1-2):265-272.
[7] Nelson DV. Effects of residual stress on fatigue crack propagation. In: Residual stress effects in fatigue, ASTM STP 776 Philadelphia: ASTM, 1982, pp. 172-187.
[8] Leitao VMA. Applications of multi-region Trefftz-collocation to fracture mechanics. Engineering Analysis with Boundary Elements 1998;22(3):251-256.
[9] Edwards L, Fitzpatrick ME, Irving PE, Sinclair I, Zhang X, Yapp D. An integrated approach to the determination and consequences of residual stress on the fatigue performance of welded aircraft structures. J ASTM Intl 2005;3(2):JAI12547.
[10] Edwards L. Influence of residual stress redistribution on fatigue crack growth and damage tolerant design Mater Sci Forum 2006;524-525:363-372.
[11] Fukuda S, Tsuruta Y. An experimental study of redistribution of welding residual stress. Trans JWRI 1978;7:67.
[12] Galatolo R, Lanciotti A. Fatigue crack propagation in residual stress fields of welded plates. International Journal of Fatigue 1997;19(1):43-49.
[13] Lam YC, Lian KS. The Effect of Residual-Stress and its Redistribution on Fatigue. Theoretical and Applied Fract Mech 1989;12(1):59-66.
[14] Lee Y-B, Chung C-S, Park Y-K, Kim H-K. Effects of redistributing residual stress on the fatigue behavior of ss330 weldment. International Journal of Fatigue 1998;20(8):565-573.

[15] Bussu G, Irving PE. The role of residual stress and heat affected zone properties on fatigue crack propagation in friction stir welded 2024-T351 aluminium joints. Intl J Fatigue 2003;25:77-88.
[16] Maddox SJ. Fatigue crack propagation in weld metal and HAZ. Metal Construction 1970;2(7):285-289.
[17] Masuda C, Sumiyoshi H, Kosuge M, Ohta A, Nishijima S. Variation of fractographic appearance for different microstructures in welded joints having the same fatigue crack propagation properties. International Journal of Fatigue 1987;9(4):233-237.
[18] Parry M, Hertzberg RW, Nordberg H. Fatigue crack-propagation in A514 base plate and welded-joints. Welding Journal 1972;51(10):485-490.
[19] Fitzpatrick ME, Edwards L. Fatigue Crack / Residual Stress Interactions and their Implications for Damage Tolerant Design. J Mater Engng Performance 1998;7(2):190-198.
[20] Allen AJ, Hutchings MT, Windsor CG, Andreani C. Neutron Diffraction Methods For the Study of Residual Stress Fields. Advances in Physics 1985;34(4):445 - 473.
[21] Fitzpatrick ME, Lodini A, editors. Analysis of Residual Stress using Neutron and Synchrotron Radiation. London: Taylor & Francis, 2003.
[22] Withers PJ, Bhadeshia HKDH. Residual stress Part 1 - Measurement techniques. Mater Sci Technol 2001;17:355-365.
[23] Bouchard PJ, George D, Santisteban JR, Bruno G, Dutta M, Edwards L, Kingston E, Smith DJ. Measurement of the residual stresses in a stainless steel pipe girth weld containing long and short repairs. International Journal of Pressure Vessels and Piping 2005;82(4):299-310.
[24] Carr DG, Ripley MI, Holden TM, Brown DW, Vogel SC. Residual stress measurements in a zircaloy-4 weld by neutron diffraction. Acta Materialia 2004;52(14):4083-4091.
[25] Ganguly S, Fitzpatrick ME, Edwards L. Use of neutron and synchrotron X-ray diffraction for evaluation of residual stresses in a 2024-T351 Aluminum Alloy Variable-Polarity Plasma-Arc weld. Metall Mater Trans 2006;37A:411-420.
[26] Ganguly S, Stelmukh V, Edwards L, Fitzpatrick ME. Measurement of residual stresses in MIG-welded Al-2024 using neutron and synchrotron X-ray diffraction. Mater Sci Engng 2008;491(1-2):248-257.
[27] Stelmukh V, Edwards L, Santisteban JR, Ganguly S, Fitzpatrick ME. Weld Stress Mapping using Neutron and Synchrotron X-ray Diffraction. Mater Sci Forum 2002;404/407:599-604.
[28] Fitzpatrick ME, Kennard MJ, Small CJ. Problems in Residual Stress Determination for Thick Components. 6th Intl Conf on Residual Stresses, Vol. 2 Oxford, UK: Institute of Materials, UK, 2000, pp. 939-946.
[29] Krawitz AD, Winholtz RA. Use of Position-dependent stress-free standards for diffraction stress measurements. Materials Science and Engineering 1994;A185:123-130.
[30] Liljedahl CDM, Tan ML, Zanellato O, Ganguly S, Fitzpatrick ME, Edwards L. Evolution of residual stresses with fatigue loading and subsequent crack growth in a welded aluminium alloy middle tension specimen. Engineering Fracture Mechanics 2008;75(13):3881-3894.
[31] Liljedahl CDM, Zanellato O, Edwards L, Fitzpatrick ME. Evolution of Residual Stresses with Fatigue Crack Growth in a Variable Polarity Plasma Arc–Welded

Aluminum Alloy Compact Tension Specimen. Metallurgical and Materials Transactions A 2008;39(10):2370-2377.
[32] Liljedahl CDM, Tan ML, Edwards L, Fitzpatrick ME. The effect of residual stress on fatigue crack growth rate in standard test samples sectioned from a VPPA-welded aluminium plate. submitted to Theoretical Applied Fracture Mechanics 2008.
[33] Pirling T, Bruno G, Withers PJ. SALSA--A new instrument for strain imaging in engineering materials and components. Materials Science and Engineering: A 2006;437(1):139-144.
[34] Bragg WL. The diffraction of short electromagnetic waves by a crystal. Proc Phil Soc 1914;17:43-57.
[35] Daymond MR, Bourke MAM, Vondreele RB, Clausen B, Lorentzen T. Use of Rietveld refinement for elastic macrostrain determination and for evaluation of plastic strain history from diffraction spectra. Journal of Applied Physics 1997;82(4):1554-1562.
[36] Holden TM, Suzuki H, Carr DG, Ripley MI, Clausen B. Stress measurements in welds: Problem areas. Materials Science and Engineering: A 2006;437(1):33-37.
[37] Stelmukh V, Edwards L, Ganguly S. Full stress tensor determination in a textured aerospace aluminium alloy plate using synchrotron X-ray diffraction. Textures and Microstructures 2003;35(3/4):175-183.
[38] Lefebvre F, Ganguly S, Sinclair I. Micromechanical aspects of fatigue in a MIG welded aluminium airframe alloy: Part 1. Microstructural characterization. Materials Science and Engineering A 2005;397(1-2):338-345.
[39] Tsakalakos T, Croft MC, Jisrawi NM, Holtz RL, Zhong Z. Measurement of Residual Stress Distributions by Energy Dispersive X-ray Diffraction Synchrotron Radiation. Sixteenth International Offshore And Polar Engineering Conference. Ayer R, Chung JS, Ames N, Wheat HG, editors. San Francisco, USA: International Society of Offshore and Polar Engineers, 2006, pp. 57-64.
[40] Croft M, Zhong Z, Jisrawi N, Zakharchenko I, Holtz RL, Skaritka J, Fast T, Sadananda K, Lakshmipathy M, Tsakalakos T. Strain profiling of fatigue crack overload effects using energy dispersive X-ray diffraction. International Journal of Fatigue 2005;27(10-12):1408-1419.
[41] Hill MR. Modeling of Residual Stress Effects using Eigenstrain. In: Presented at ICF10, Hawaii, 2001, 2001, p. http://mae.ucdavis.edu/~mhill/papers/Hill_ICF10979OR.pdf.
[42] DeWald AT, Hill MR. Multi-Axial contour method for mapping residual stresses in continuously-processed bodies. Experimental Mechanics 2006;46(4):473-490.
[43] Bueckner HF. The propagation of cracks and the energy of elastic deformation. Trans ASME 1958;80:1225-1230.
[44] Kanazawa T, Oba H, Machida S. Society of Naval Architects of Japan Journal 1961;109:359-369.
[45] Rice J. A path independent integral and approximate analysis of strain concentration by notches and cracks. J Appl Mech 1968;35:379-387.
[46] Liljedahl CDM, Brouard J, Zanellato O, Lin J, Tan ML, Ganguly S, Irving PE, Fitzpatrick ME, Zhang X, Edwards L. Weld residual stress effects on fatigue crack growth behaviour of aluminium alloy 2024-T351. International Journal of Fatigue;In Press, Corrected Proof.

[47] Parker P. Linear elastic fracture mechanics and fatigue crack growth. Residual Stress and Stress Relaxation, Proceedings of the 28th Sagamore Army Materials Research Conference Lake Placid, New York, 1982, pp. 249-271.
[48] Harter JA. AFGROW Users Guide and Technical Manual. Ohio, USA: Air Force Research Laboratory, 2004.

FIGURE CAPTIONS

Fig. 1 Schematic and dimensions of the M(T) geometry specimens. (WP: weld pool, NHAZ: near heat-affected zone, FHAZ: far heat-affected zone). The heat-affected zone extended on average about 15 mm either side of the weld centre.

Fig. 2 Set-up at the SALSA diffractometer for measurement of the longitudinal strain direction in the M(T) specimen

Fig. 3 Variation of 2θ in the comb with distance from the weld centre

Fig. 4 Measured residual a) strains and b) stresses along the un-cracked path in the M(T) specimen

Fig. 5 Residual stresses in the longitudinal direction at crack lengths a of: a) 0, 3 mm, b) 7, 9 mm, c) 11, 13 mm, d) 15, 17 mm and e) 19, 21. The crack length values have been averaged and rounded for clarity, although the crack growth was found to be highly symmetric.. Modelled data are also plotted, and are discussed in section 4. The number in the legends corresponds to the crack length in mm. The 0 legend points correspond to the data measured along the un-cracked path.

Fig. 6 Comparison between the longitudinal stresses in the unloaded condition and at P_{max} at crack lengths of a) 7 mm and b) 20 mm, for both measured and modelled results. Data is shown for the residual stress with no load (RS); residual stress plus applied load (P + RS); and for the effects of the load (obtained directly from the FEA, and by subtracting the difference between the loaded and unloaded experimental data.

Fig. 7 Experimentally measured fatigue crack growth rate in the M(T) specimen. The experimental data is also compared with the prediction of the fatigue crack growth rate, with and without taking into account the residual stresses. The procedures for the predictions are explained in section 5.2.

Fig. 8 Modelled and measured initial un-cracked stress distribution in the longitudinal direction

Fig. 9 Mesh convergence of stresses averaged over the gauge volume (at 17 mm crack length).

Fig. 10 Evolution of K_{res} with crack position from the weld centre for the M(T) specimen (comparison between FEA and weight function approaches)

Fig. 11 a) Applied ΔK and b) Evolution of the effective R with crack growth from the weld centre for the M(T) specimen

Figure 1

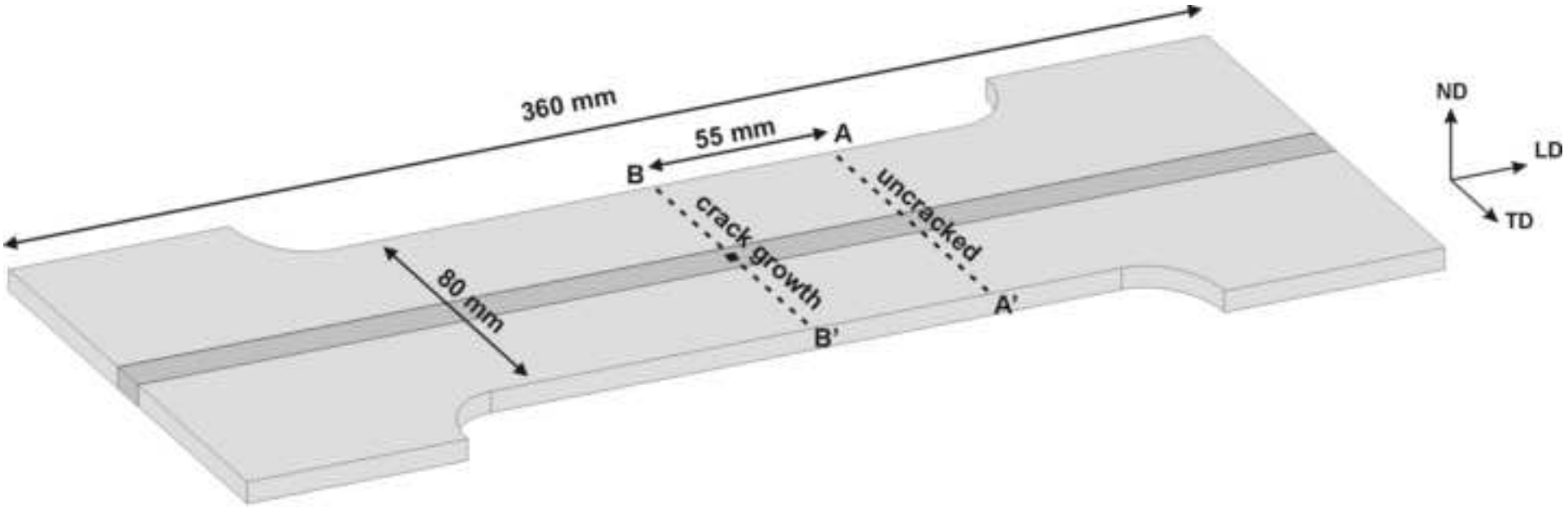

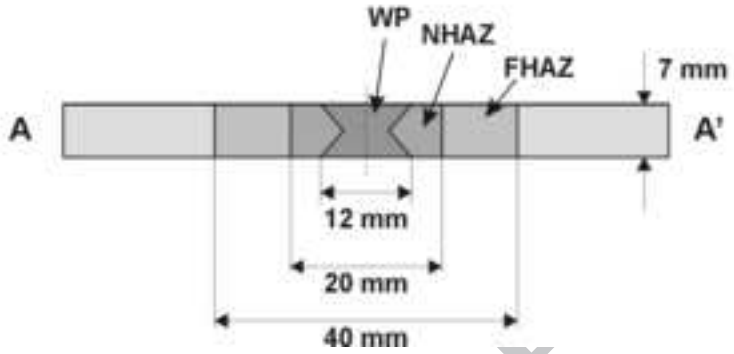

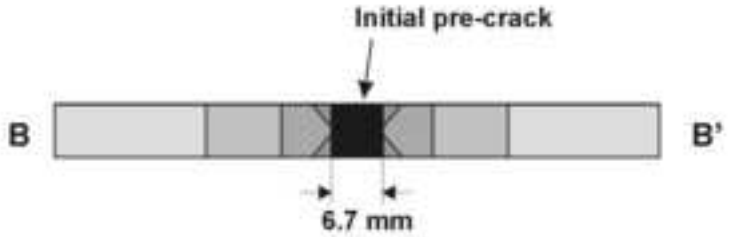

Figure 2

Figure 3

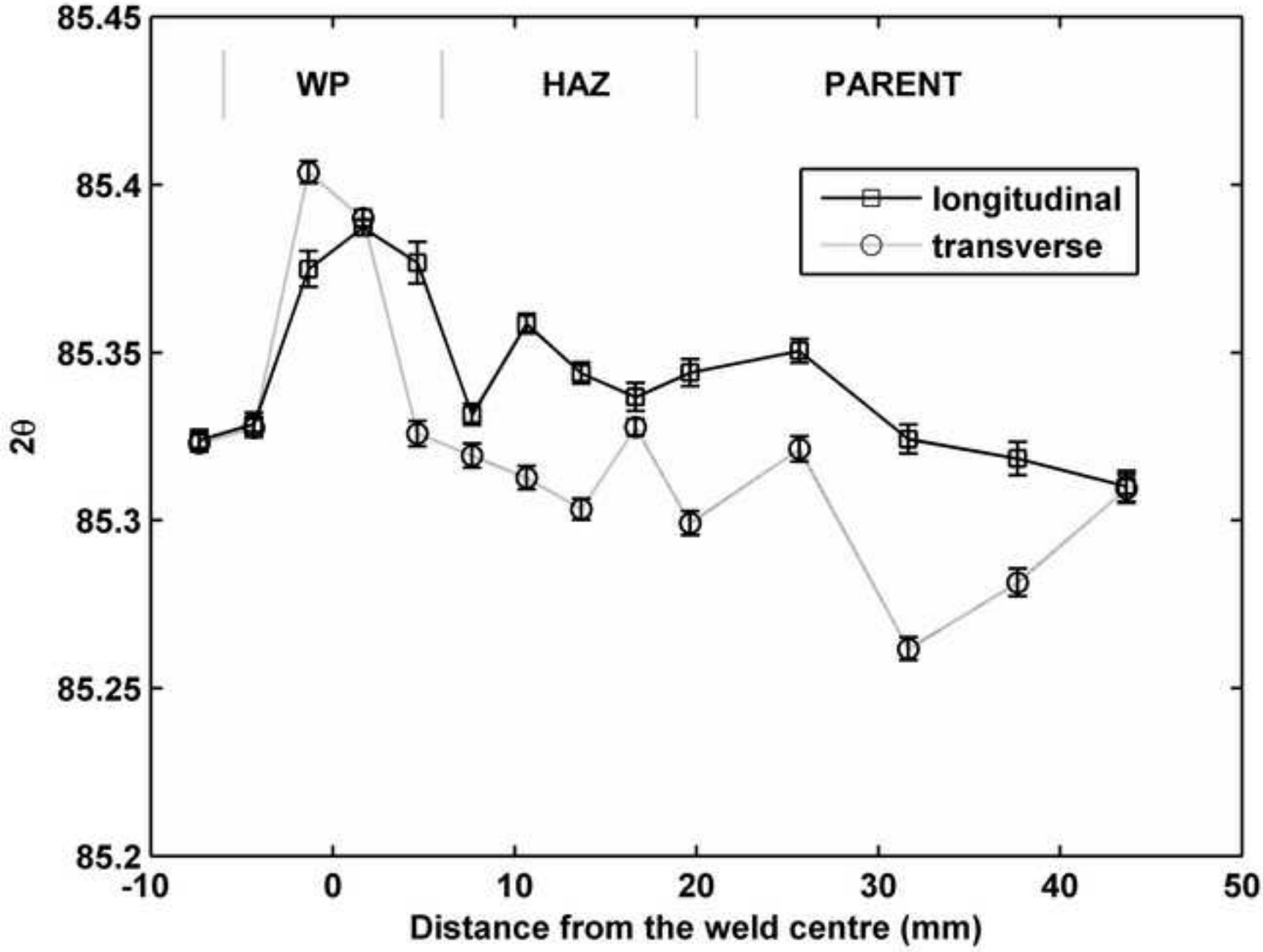

Figure 4a

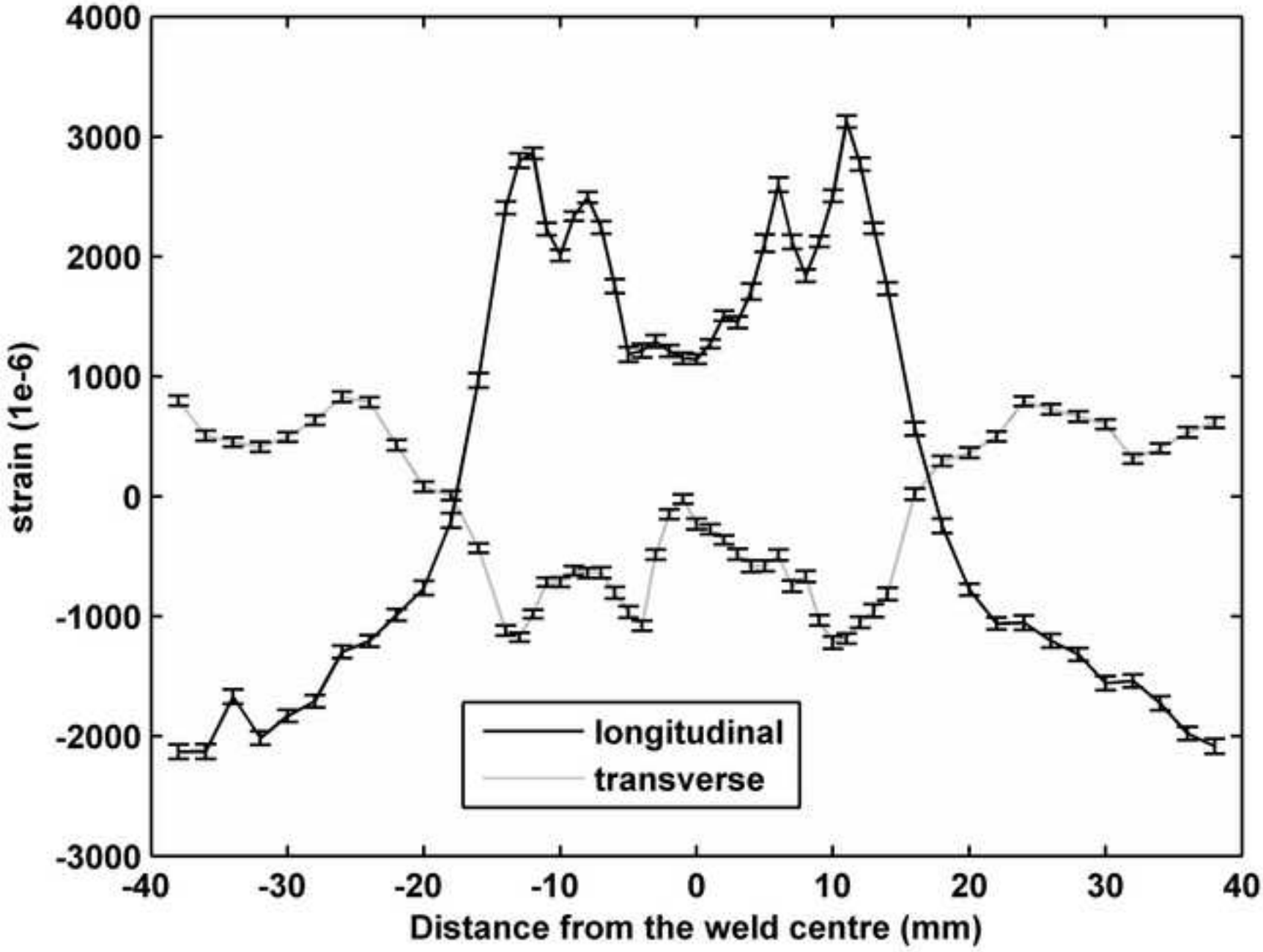

Figure 4b

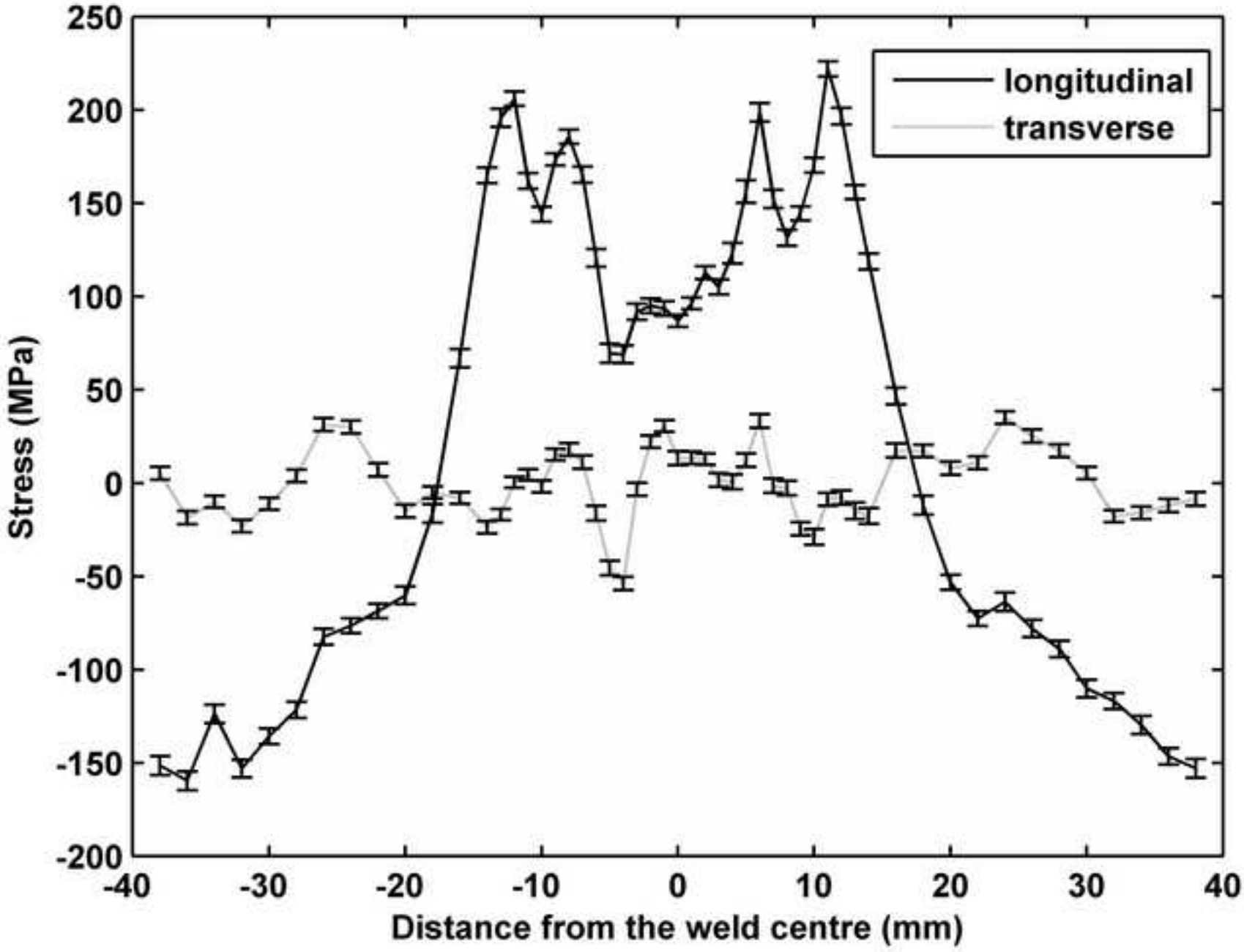

Figure 5a

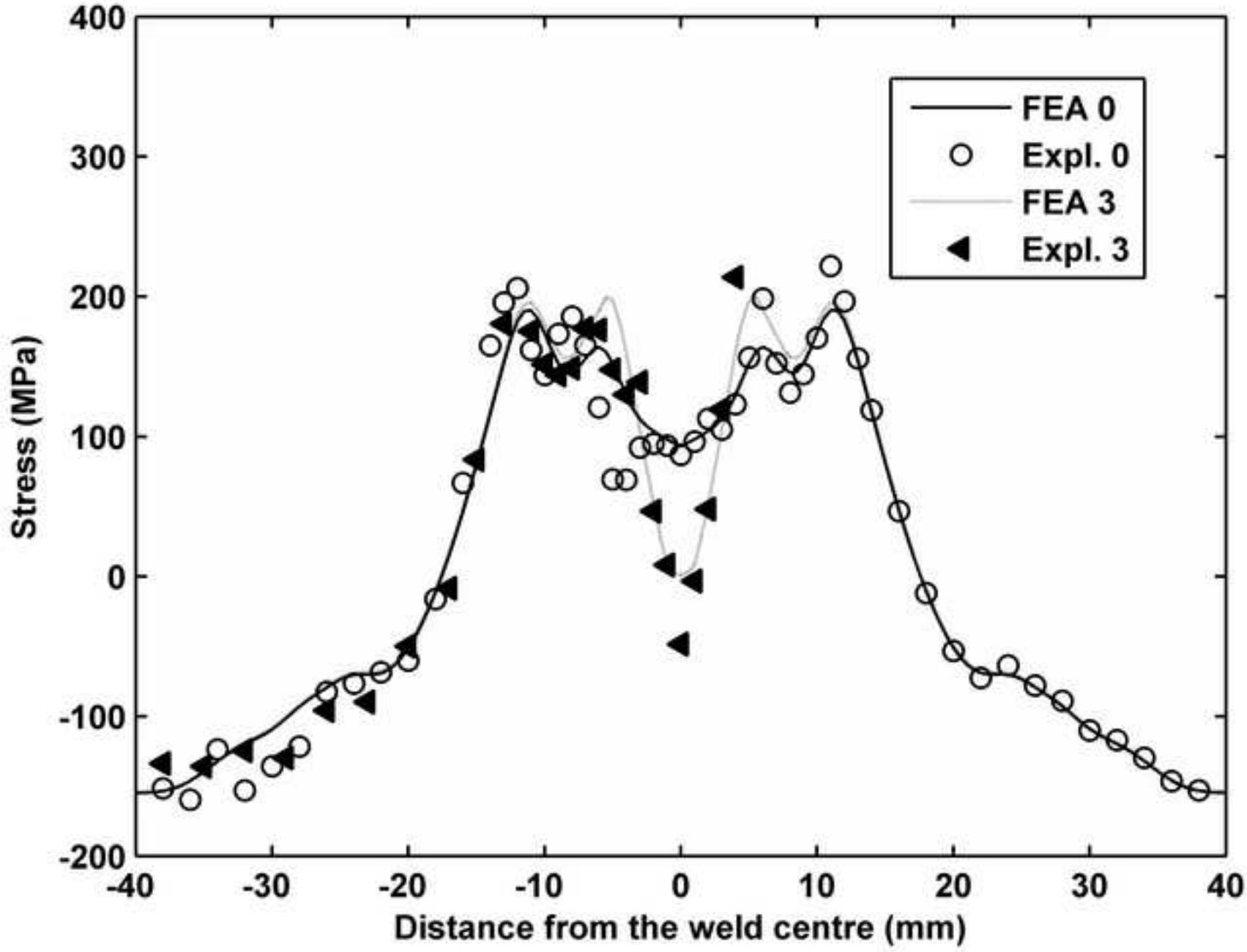

Figure 5b

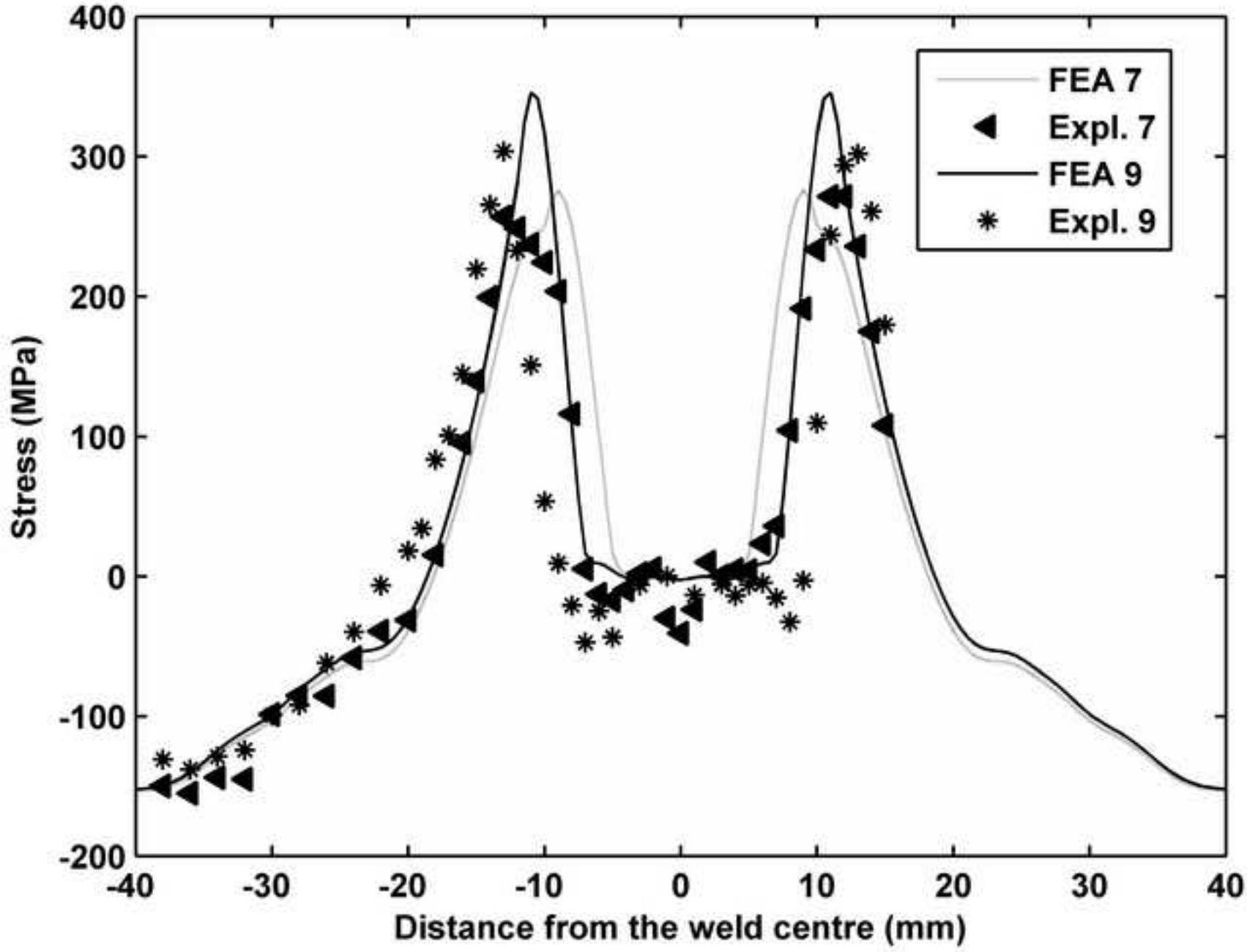

Figure 5c

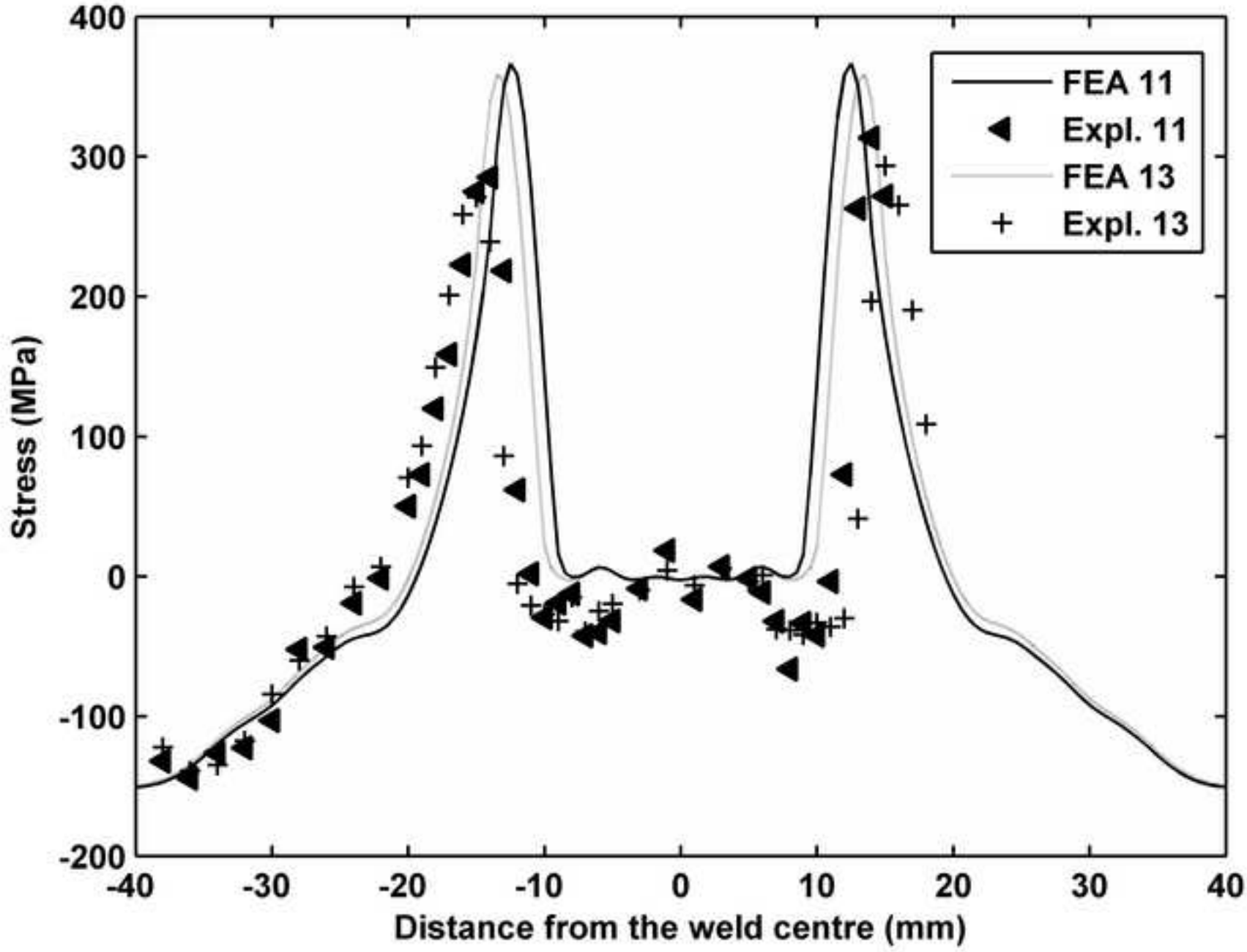

Figure 5d

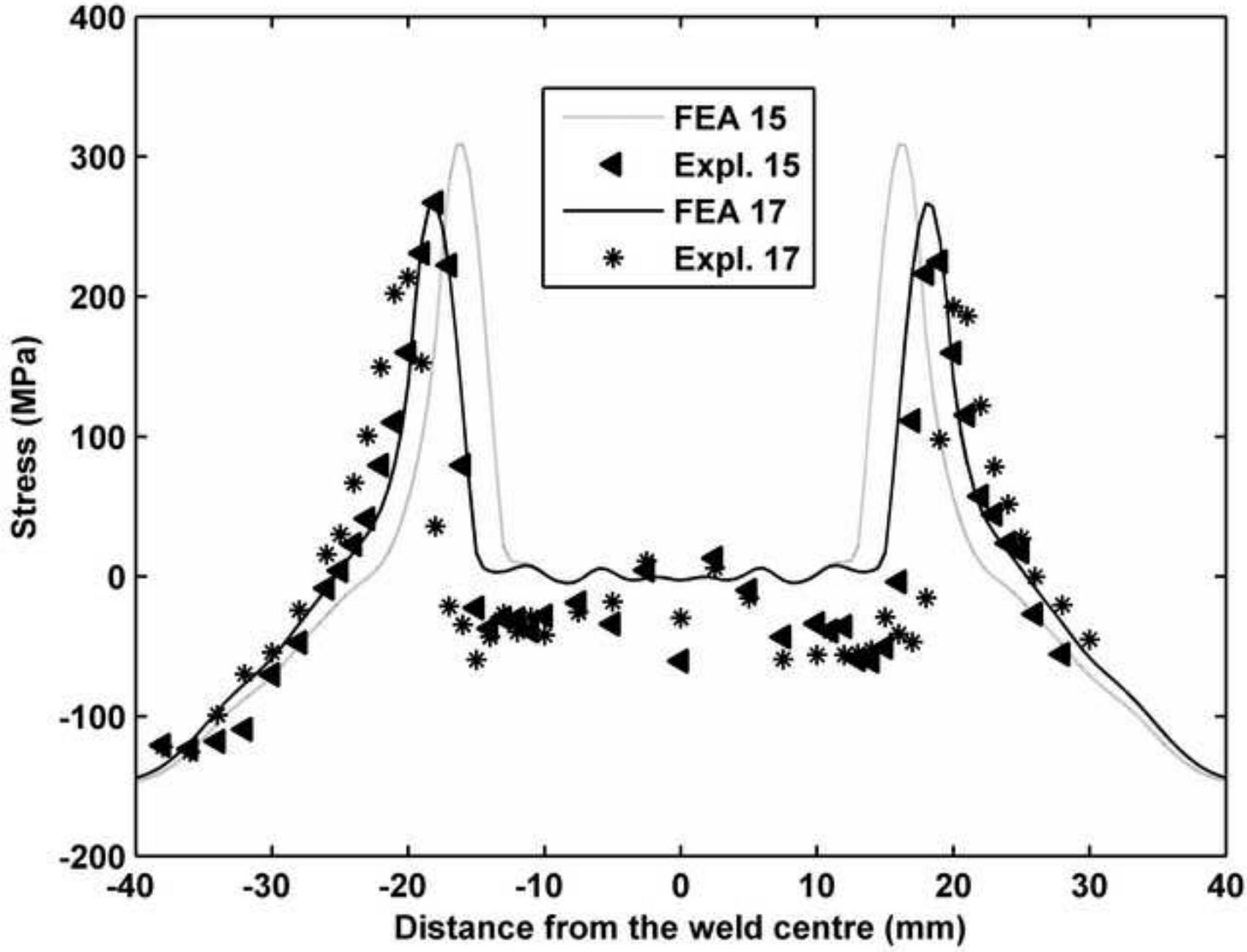

Figure 5e

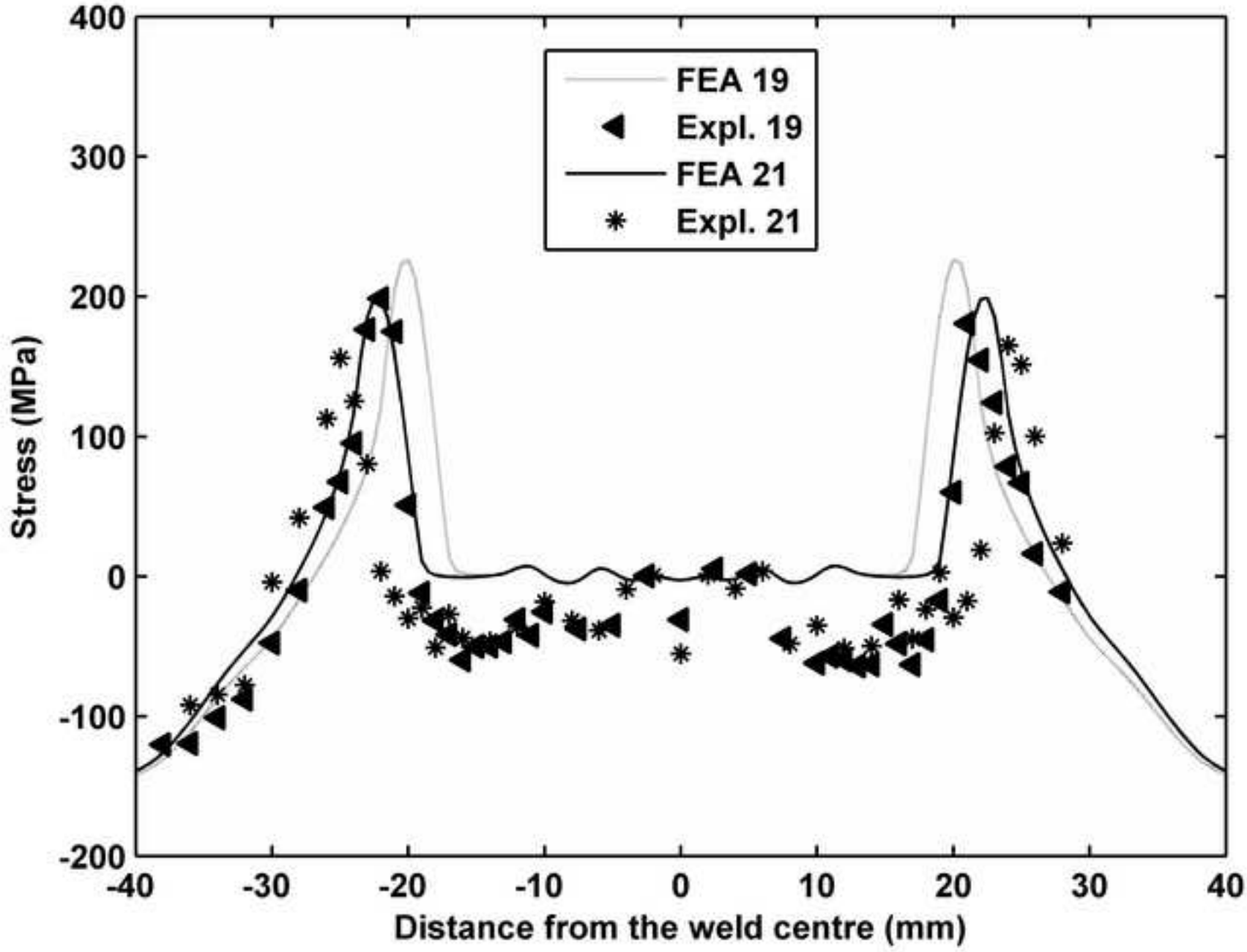

Figure 6a

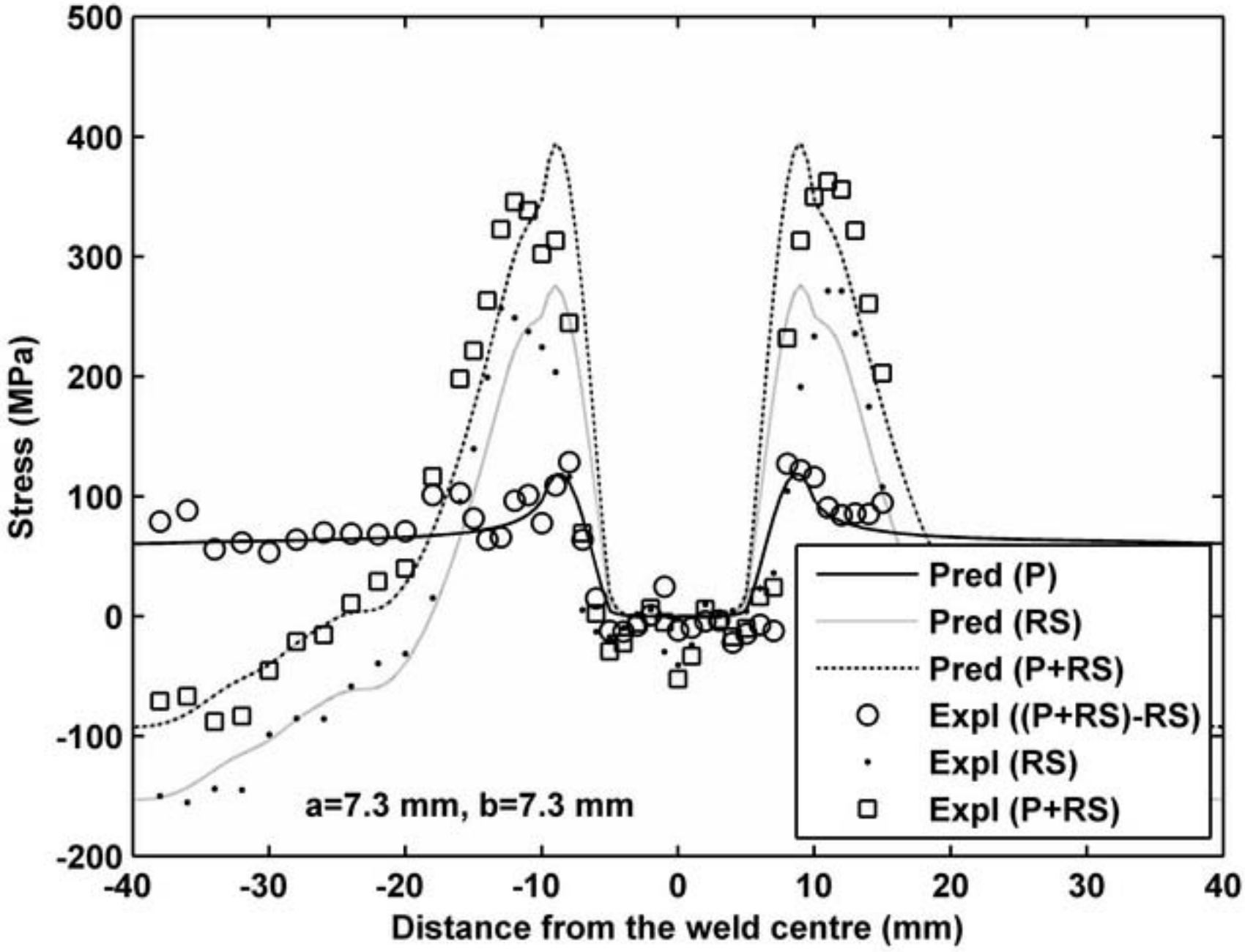

Figure 6b

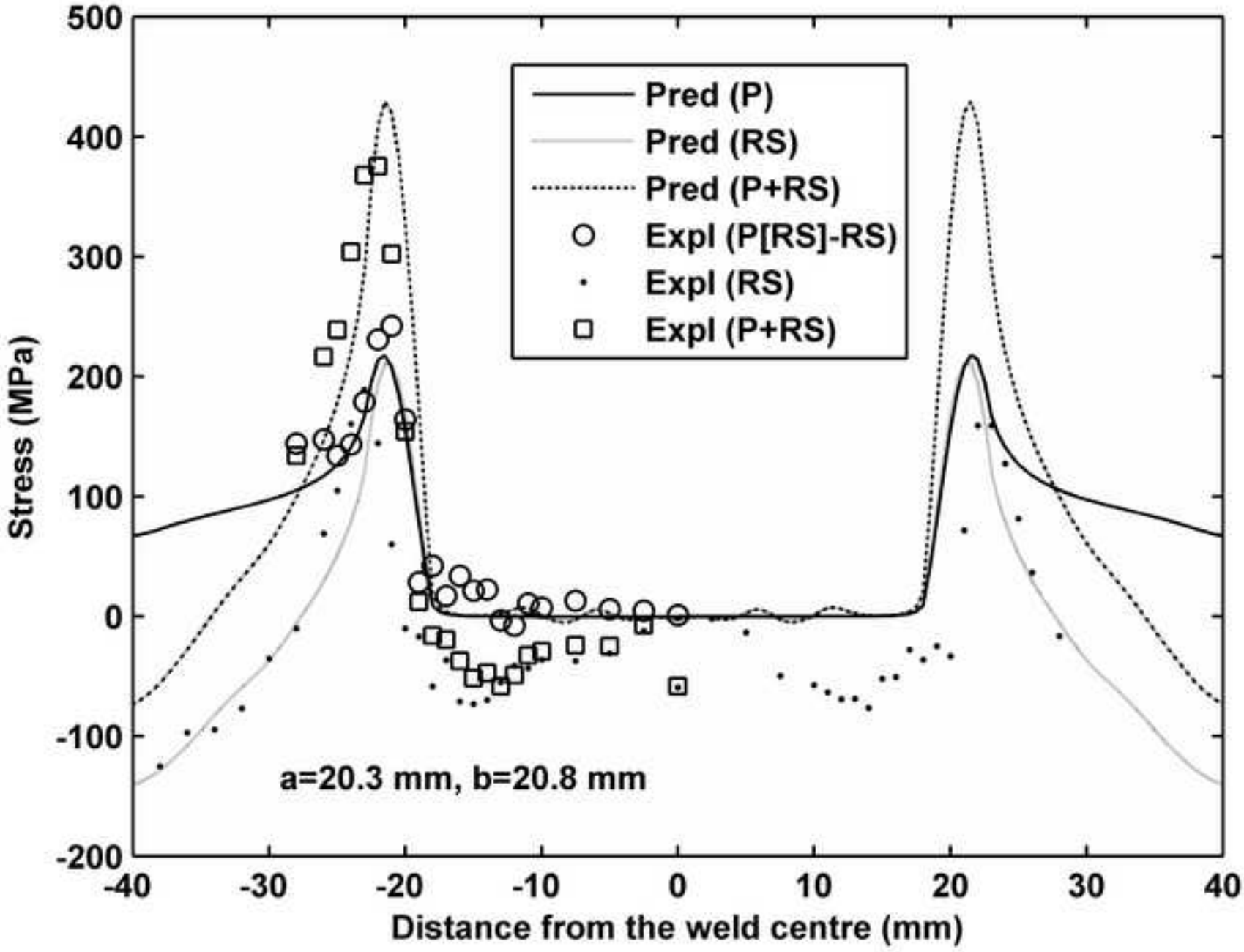

Figure 7

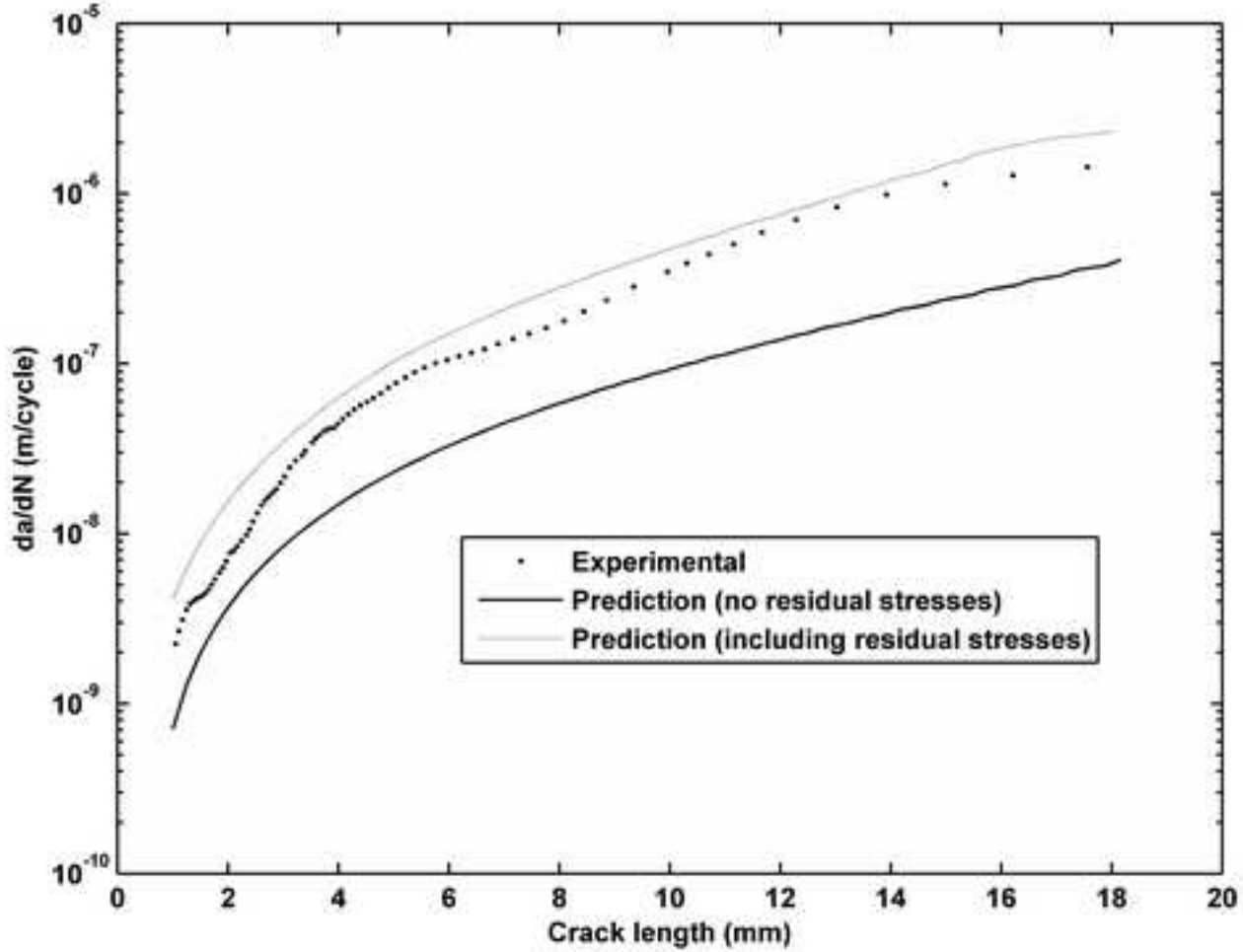

Figure 8

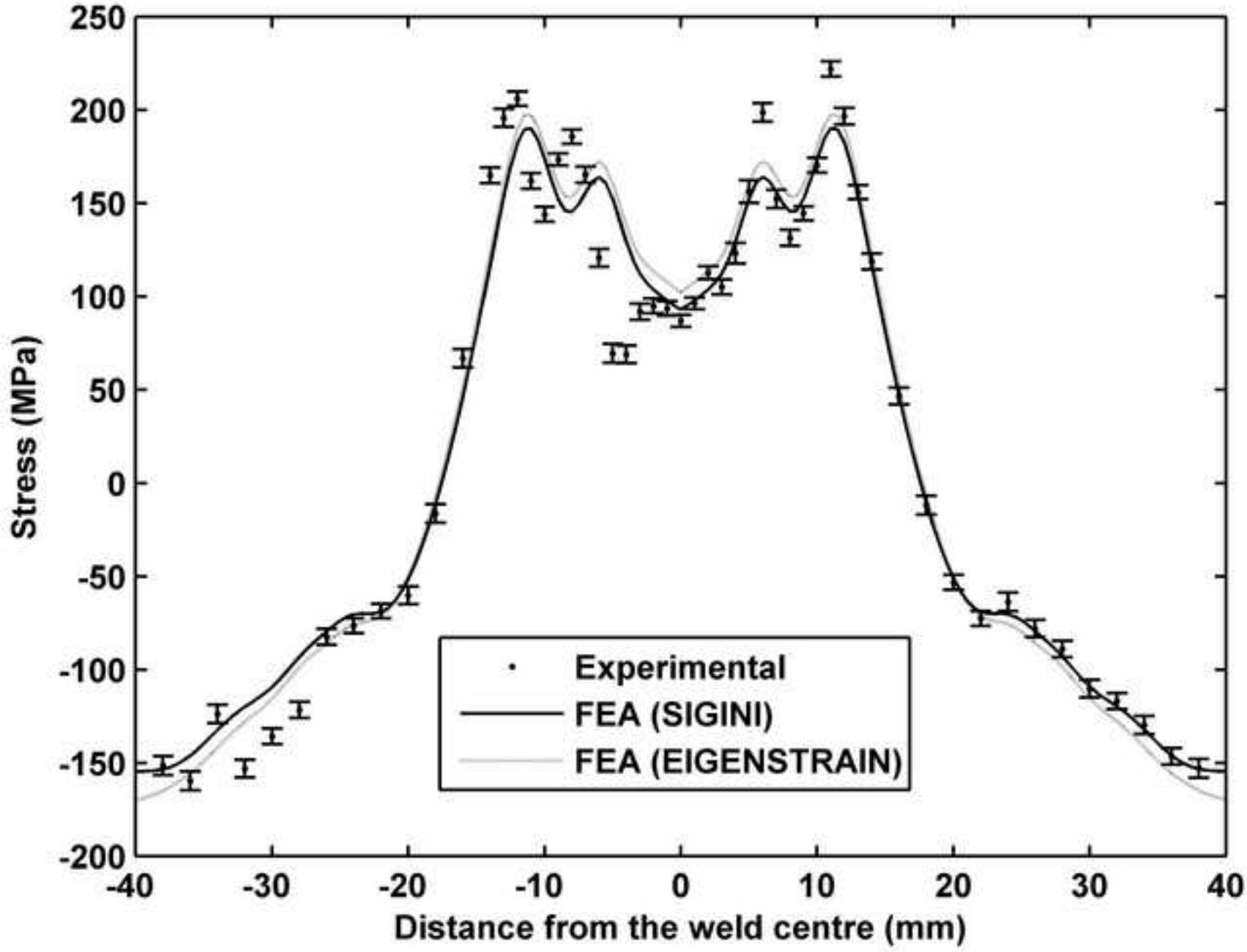

Figure 9

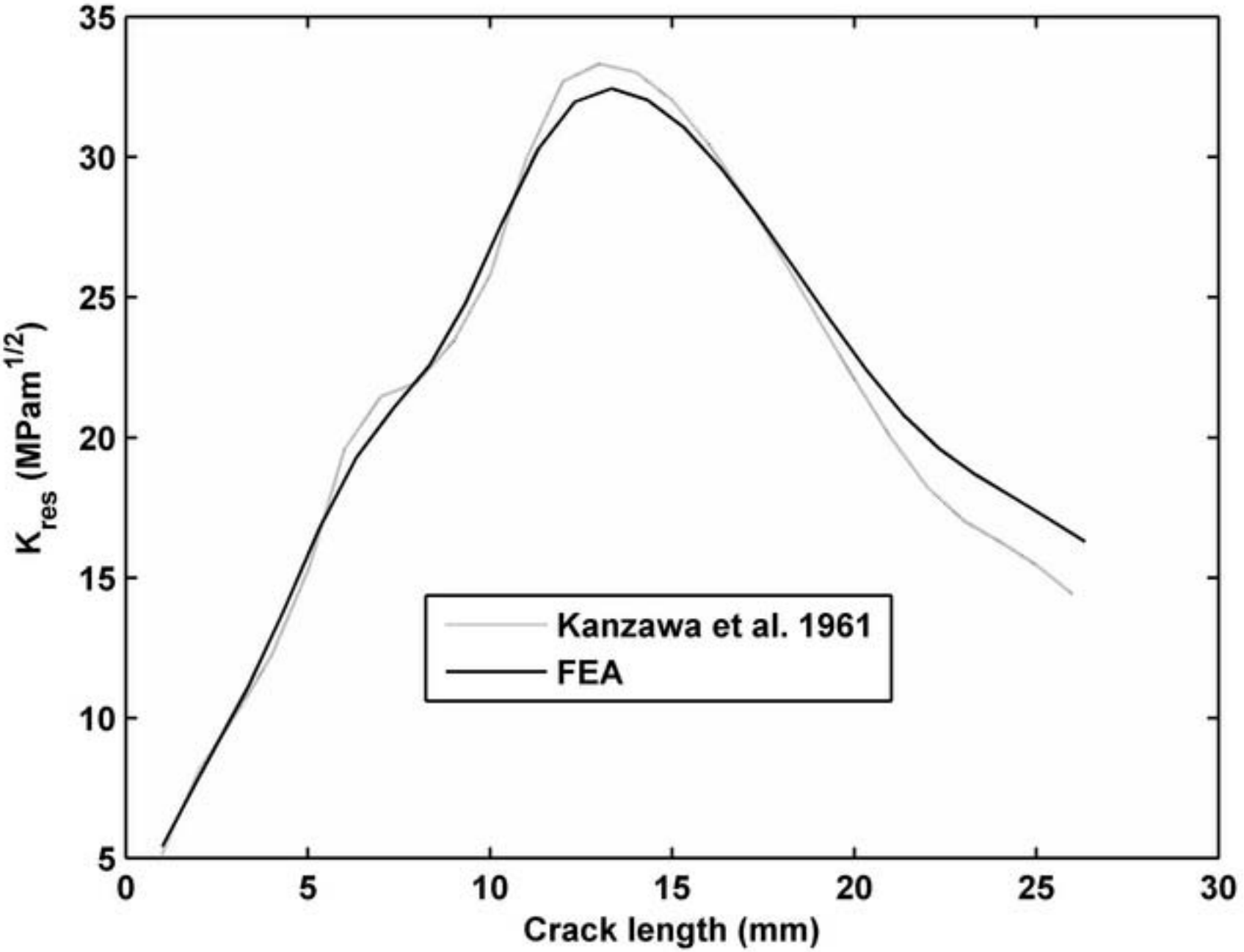

Figure 10

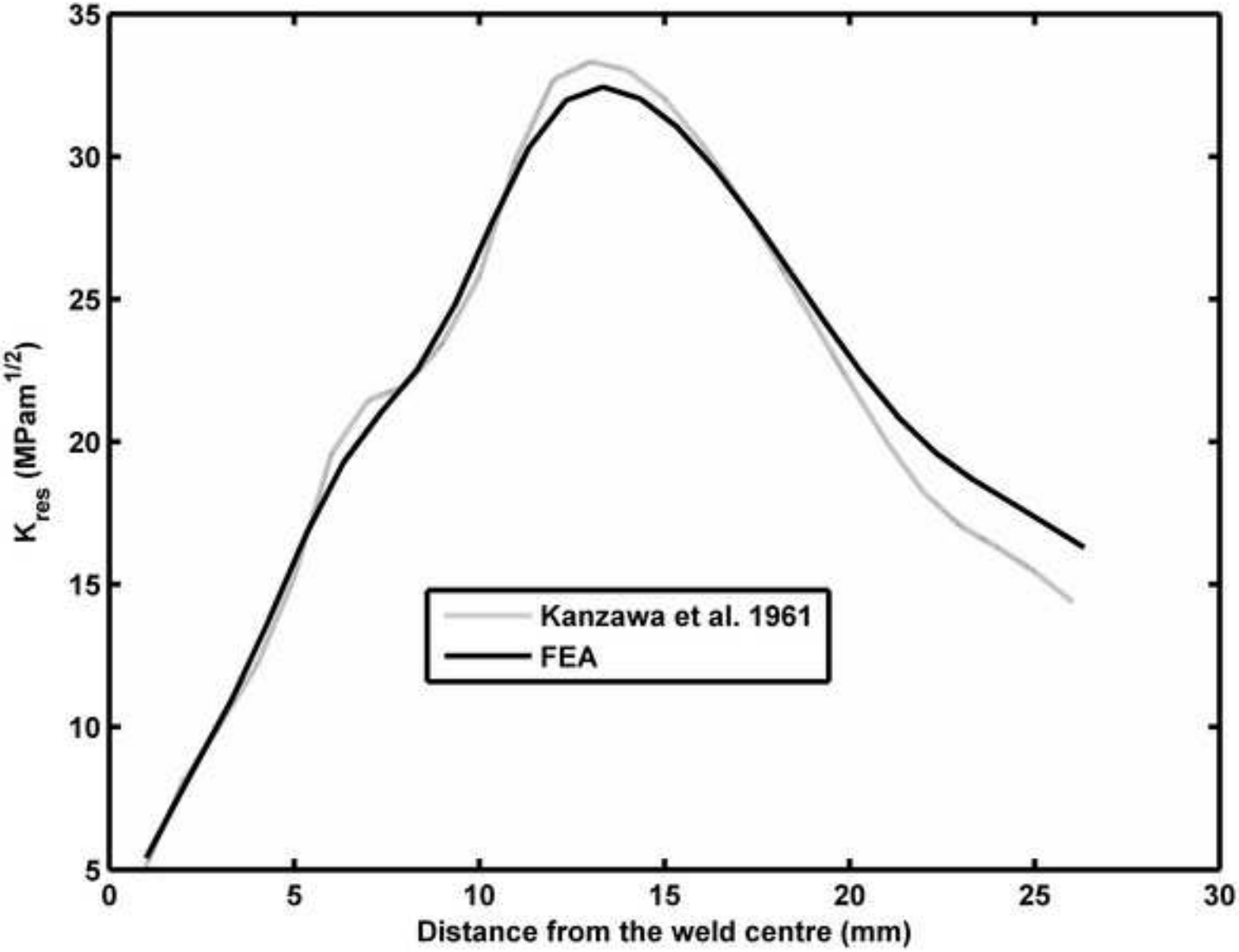

Figure 11a

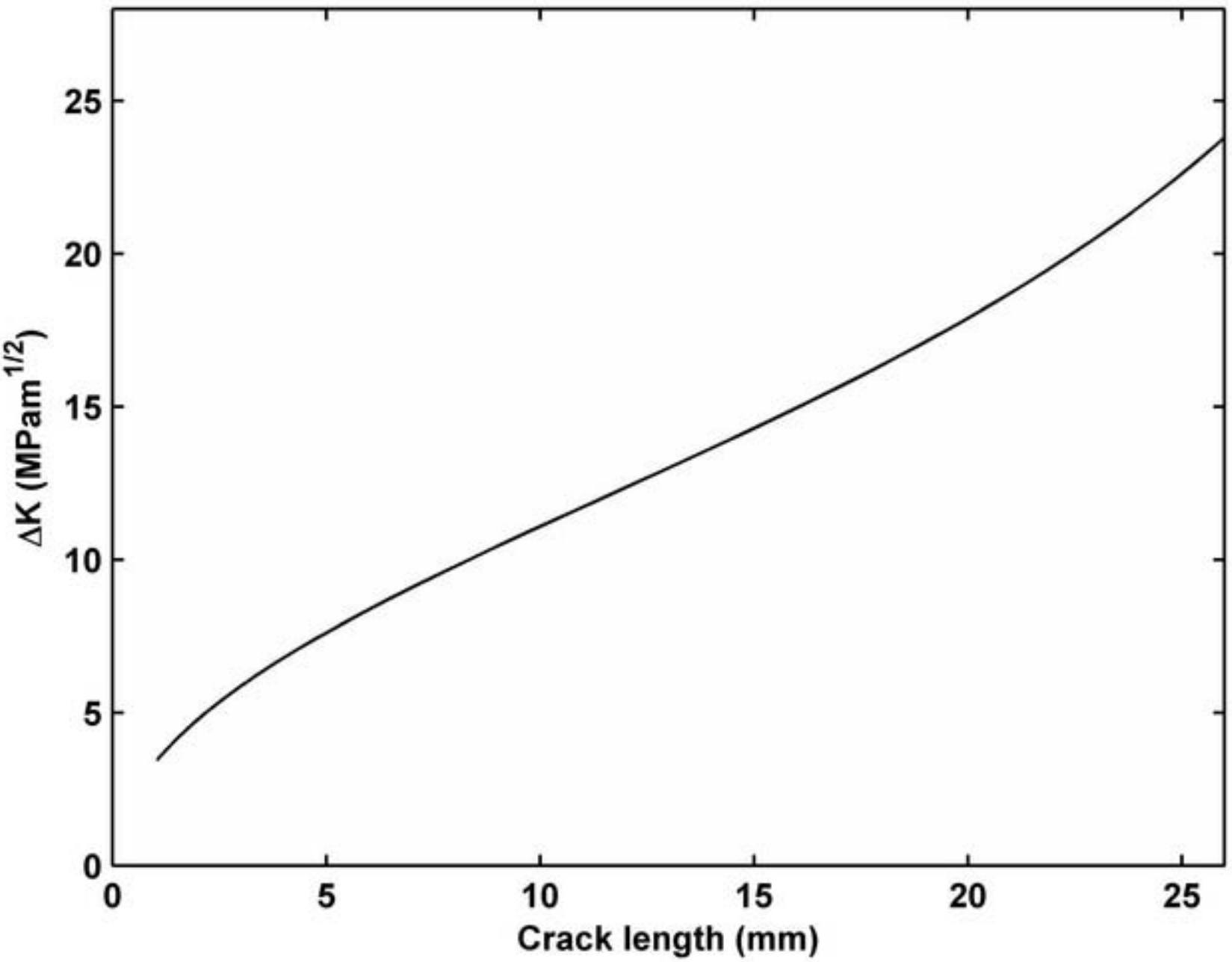

Figure 11b